Journal of Colloid and Interface Science 585 (2021) 184–194

Contents lists available at ScienceDirect

Journal of Colloid and Interface Science

journal homepage: www.elsevier.com/locate/jcis

Regular Article

Fast-dissolving antibacterial nanofibers of cyclodextrin/antibiotic inclusion complexes for oral drug delivery

Fuat Topuz [a,*], Mehmet E. Kilic [b], Engin Durgun [c], Gyorgy Szekely [a,*,1]

[a] Advanced Membranes and Porous Materials Center, Physical Science and Engineering Division (PSE), King Abdullah University of Science and Technology (KAUST), Thuwal 23955-6900, Saudi Arabia
[b] Department of Materials Science and Engineering, Yonsei University, 03722 Seoul, Republic of Korea
[c] UNAM-National Nanotechnology Research Center, Bilkent University, Ankara 06800, Turkey

HIGHLIGHTS

- Polymer-free CD@antibiotic inclusion complex nanofibers were prepared by electrospinning.
- Bead-fee nanofibers could be produced at two different molar ratios of four antibiotics.
- The inclusion-complexation with CD drastically enhanced the water solubility of antibiotics.
- The formation of inclusion-complexation was also confirmed by *ab initio* modeling studies.
- The nanofibers rapidly dissolve in artificial saliva, releasing CD@antibiotic complexes.

GRAPHICAL ABSTRACT

ARTICLE INFO

Article history:
Received 9 October 2020
Revised 9 November 2020
Accepted 19 November 2020
Available online 24 November 2020

Keywords:
Electrospinning
Cyclodextrin
Inclusion complex (IC)
Antibacterial nanofibers
Antibiotics
Oral drug delivery

ABSTRACT

Hypothesis: The widespread use of antibacterial electrospun nanofibers is mostly restricted due to their low loading capacity to carry antibiotics and the need to use toxic organic solvents to boost the antibiotic loading capacity. Nanofibers based on natural excipients, such as cyclodextrin (CD)-based nanofibers, can carry -larger amounts of antibiotics while achieving better stability *via* inclusion complexation.
Experiments: Nanofibers were produced by electrospinning and analyzed by electron microscopy to investigate the morphology of fibers. The formation of inclusion-complexation was analyzed by ^{1}H NMR, FTIR, and XRD. Thermal analysis of the fibers was done using TGA. *Ab initio* modeling studies were done to calculate the complexation energies of antibiotics with CD. A disk-diffusion assay was used to test the antibacterial activity of the fibers.
Findings: Bead-free antibacterial nanofibers with mean diameters between 340 and 550 nm were produced. The formation of inclusion complexes (IC) between the CD and the antibiotics was confirmed by FTIR and ^{1}H NMR, which was further verified by the disappearance of the crystalline peaks of antibiotics as determined by XRD analysis. Thermal analysis of the nanofibers revealed that the formulations showed good antibiotic encapsulation (45–90%). *Ab initio* simulations revealed that gentamicin had the highest complexation energy, followed by kanamycin, chloramphenicol, and ampicillin. The antibacterial nanofibers rapidly dissolved in water and artificial saliva, successfully releasing the CD antibiotic complexes. The nanofibers showed high antibacterial activity against Gram-negative *Escherichia coli*.

* Corresponding authors.
E-mail addresses: fuat.topuz@kaust.edu.sa (F. Topuz), gyorgy.szekely@kaust.edu.sa (G. Szekely).
URL: http://www.szekelygroup.com (G. Szekely).
[1] www.szekelygroup.com

https://doi.org/10.1016/j.jcis.2020.11.072
0021-9797/

1. Introduction

Cyclodextrin (CD) is a cyclic oligosaccharide formed through an intramolecular transglycosylation reaction during the enzyme-mediated degradation of starch [1]. CD has a unique toroidal shape with a partially hydrophobic cavity interior and a hydrophilic exterior. CD molecules can host organic and inorganic molecules in their hydrophobic cavities, enabling their use as solubilization enhancers for various poorly water-soluble drug molecules [2–6]. This property has also been exploited by various materials to form complexes with drugs, pollutants, and targeted molecules of interest. For instance, CD has also been employed to produce supramolecular networks through key-lock mechanisms [7–9]. Materials composed solely of CD, such as electrospun polymer-free CD fibers, are of great interest because they contain highly functional CD and have a high surface-to-volume ratio [2].

The electrospinning of CD can be performed without the need for a polymer carrier [10]. The hydrogen bonds in CD drive nanofiber formation; a similar phenomenon has recently been observed for hydrogen-bonded tannic acid aggregates [11]. Inclusion complexes (ICs) of CD with various molecules can also be electrospun into nanofibers. CD nanofibers have thus been exploited by various applications, including drug delivery [2], tissue engineering [12], catalysis [13], water treatment [14], and food engineering [15]. Antimicrobial CD nanofibers have been developed that incorporate phytochemicals and synthetic chemicals with antimicrobial activity [17]. Bio-related applications of CD nanofibers require some additional antibacterial activity because CD by itself is not antibacterial; in fact, bacteria can utilize and consume CD as a carbon source [16]. Nanofibers incorporated with essential oils and phytochemicals have low antibacterial activity, even at high loadings of antibacterial agents with molar ratios of 1:1 or 1:2 relative to the CD content. Therefore, the entrapment of highly potent antibiotics in nanofibers at lower ratios (*e.g.*, 1:0.05) is sought so that the uncomplexed CD can carry drug molecules *via* inclusion complexation.

Because the cavity interior is partially hydrophobic, the IC increases the indirect water solubility of antibiotics. Moreover, the shielding effect of the CD cavity also protects the antibiotics against harsh surrounding conditions. Thus, polymer-free CD fibers spun from water have great potential in oral drug delivery, such as orally administered CD fibers with IC-incorporated antibiotics.

In this study, we produce an oral delivery system of antibiotics based on electrospun CD@antibiotics nanofibers. We produce aqueous HP-β-CD solutions with various incorporated antibiotics (Fig. 1). We optimize the CD concentration to obtain ultrafine fibers for each antibiotic system, and we explore the IC between the CD and antibiotics through ^{1}H NMR and XRD analyses. The FTIR and TGA analyses verify the presence of the antibiotics in the fibers. Furthermore, *ab initio* simulations confirm the formation of ICs between the CD and the individual antibiotic molecules in a vacuum and in an aqueous medium. We carry out dissolution tests in water and artificial saliva. Finally, we explore the fibers' antibacterial activity through a disk diffusion assay using Gram-negative bacteria (*E. coli*).

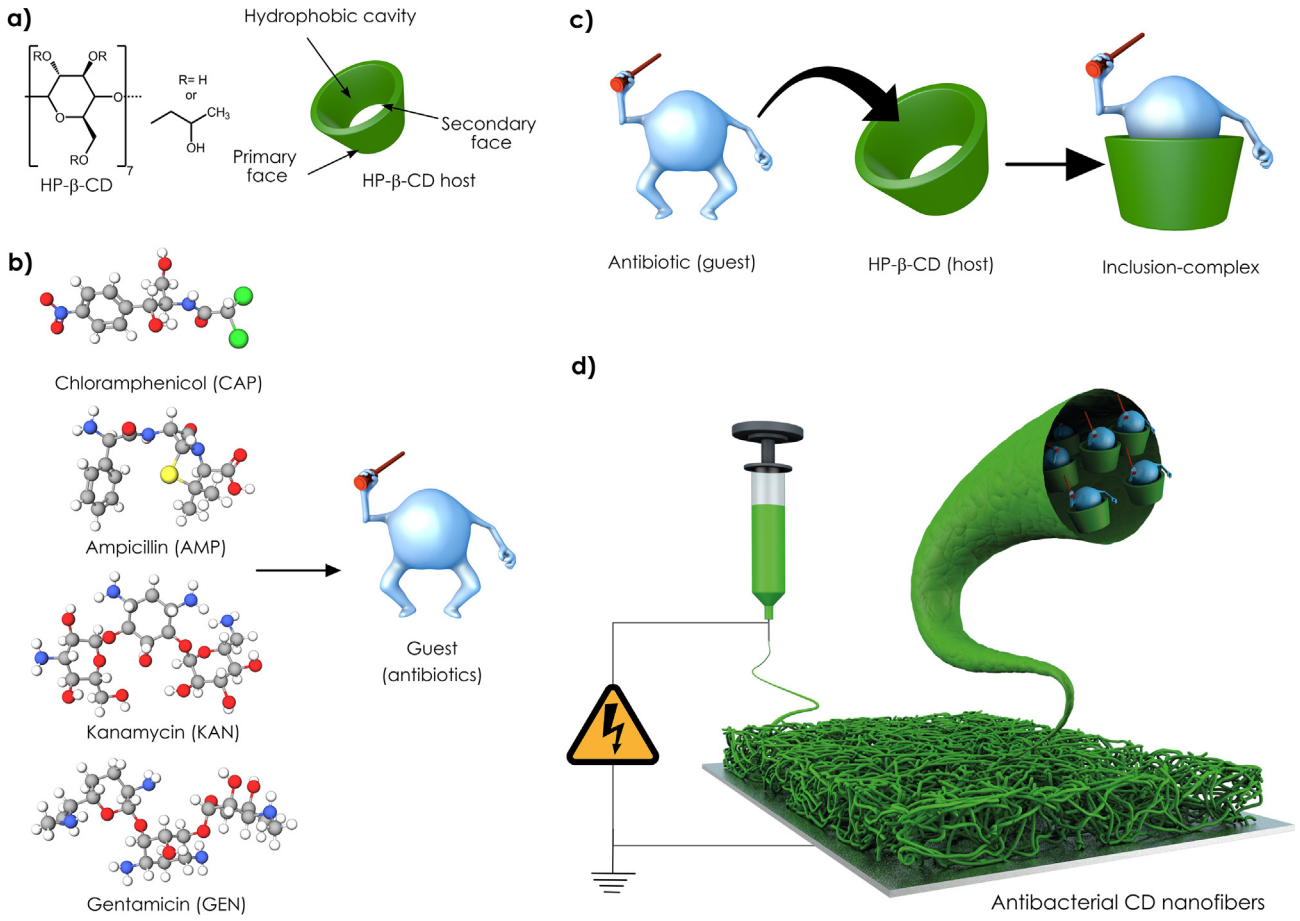

Fig. 1. The chemical structures of HP-β-CD (a) and antibiotics with high potency, namely chloramphenicol (CAP), ampicillin (AMP), kanamycin (KAN), and gentamicin (GEN) (b). Schematic for the inclusion complexation between the CD and the antibiotics (c), and the electrospinning process (d).

2. Experimental section

2.1. Materials

2-Hydroxypropyl-β-cyclodextrin (HP-β-CD) was purchased from Sigma Aldrich. The average degree of substitution was 0.8 units of 2-hydroxypropyl (C_3H_7O) per glucose unit (M_w = 1460 g mol^{-1}). Kanamycin (KAN, Fischer, 99%), chloramphenicol (CAP, Fischer, 97%), gentamicin (GEN, Sigma Aldrich), and ampicillin (AMP, Sigma Aldrich, 95%) were used as received. Na_2HPO_4 (≥99.0%, Sigma Aldrich), KH_2PO_4 (≥99.0%, Sigma Aldrich) and NaCl (99%, Fisher Scientific) were used as received. One Shot™ TOP10 Chemically Competent *Escherichia coli* (*E. coli*) (Invitrogen™) was employed for the bacterial tests. Millipore Type II water was used during the electrospinning experiments.

2.2. Electrospinning of CD nanofibers

HP-β-CD was dissolved in water and mixed with the antibiotic at respective stoichiometries of 1:0.05 and 1:1 under continuous stirring for two hours. The solution was then transferred into a 1 mL disposable plastic Normjet™ Thermo Scientific syringe equipped with a sharp-edged metallic needle (Tyco, Kendall 30G). The syringe was placed horizontally on a KD Scientific - Legato® syringe pump and discharged at a specific speed. A high-power voltage supply (SRS, Stanford Research System) was employed for the electrospinning. The nanofibers were collected on a square metal collector covered with aluminum foil. During the electrospinning process, the temperature was maintained at 21 °C, and the relative humidity was in the range of 50–55%.

2.3. Characterization

^{1}H Nuclear magnetic resonance (NMR) spectra of CD, antibiotics, and CD@antibiotics fibers were recorded on a Bruker AVANCE-III spectrometer at a frequency of 500 MHz using a sample concentration of 10 mg mL^{-1} in DMF-d7 and D_2O. The decomposition temperatures of the fiber mats and CD were measured with a TGA Q5500 (TA Instruments) at a rate of 10 °C min^{-1} and up to 700 °C. FTIR spectra of the fibers and antibiotics were recorded on Nicolet™ iS™ 10 FTIR Spectrometer equipped with a Smart Diamond ATR accessory over 128 scans with a resolution of 4 nm. The morphology of the electrospun nanofibers was explored by scanning electron microscopy (SEM) (Magellan SEM, FEI). Before SEM analysis, the fiber specimens were coated with 5 nm Pt with a sputtering system. The mean diameters of the electrospun nanofibers were determined from the respective SEM images over 100 nanofibers by ImageJ software (NIH, US National Institutes of Health). The crystal structures of the fibers and antibiotics were analyzed using X-ray diffraction (XRD, Bruker, D8 Advance) with Cu-Kα radiation.

2.4. Dissolutions tests

Dissolution tests were performed using water and artificial saliva. The artificial saliva was prepared using Na_2HPO_4 (1.19 g), KH_2PO_4 (0.095 g), and NaCl (4 g) in 500 mL distilled water. The pH of the solution was adjusted to 6.8 by adding phosphoric acid. The electrospun mats were put on the wetted tissues in a plastic petri dish, and the dissolution was recorded by a camera. Images were taken during the dissolution process at set times.

2.5. Computational modelling

Ab initio computational methods [18,19] using the framework of density functional theory (DFT) [20,21] were used to calculate the ground-state properties of the molecules. The Perdew-Burke-Ernzerhof form of generalized gradient approximation [22] was employed to determine the exchange–correlation term. The Grimme approach was used to describe the weak intermolecular forces between molecules (*i.e.*, van der Waals forces) [23]. The projector augmented-wave method [24] was implemented to describe the element potentials. During the modeling studies, each hydroxypropyl (HP) β-CD molecule was decorated with four HP units (degree of substitution: 0.6). The structural relaxations were carried out by conjugate gradient optimization, allowing 10^{-5} eV energy tolerance between two sequential steps and a maximum 0.01 eV Å^{-1} force on atoms. The implicit self-consistent description was used to analyze the interaction between the solute and solvent [25].

The interaction energy (E_{int}) is defined as

$$E_{int} = E_T(CD) + E_T(guest) - E_T(IC) \quad (1)$$

where E_T(CD), E_T(guest), and E_T(IC) are the ground-state energy of HP-β-CD, the single antibiotic molecule (for 1:1 stoichiometry), and the IC, respectively. The IC is considered to be formed when E_{int} is maximized, and the maximum value of E_{int} for the given configuration is defined as the complexation energy (E_{comp}).

Solvation energy (E_{solv}) is defined as

$$E_{solv} = E_T[IC]_{water} - E_T[IC]_{vacuum} \quad (2)$$

$E_T[IC]_{water}$ and $E_T[IC]_{vacuum}$ are the ground-state energy of antibiotic/HP-β-CD-IC in water and a vacuum, respectively.

2.6. Disk diffusion assay

The antibacterial activity of the electrospun nanofibers produced from aqueous CD solutions with different antibiotics was tested using the agar diffusion method against Gram-negative bacteria, *Escherichia coli (E. coli)* RSHM (strain TOP10), which is a commercial derivative of the more general strain DH10B). The used *E. coli* strain showed resistance to chloramphenicol. The bacteria (*E. coli*) were grown overnight, followed by a 3-fold dilution of 50 µL (6×10^8 CFU mL^{-1} of *E. coli*) bacteria with PBS buffer. The diluted bacteria were poured onto the 2X YT agar plates. Afterward, the circular fiber samples (diameter = 4.54 mm) were placed on the agar plates and incubated at 37 °C for 24 h. The widths of the inhibition zone (*i.e.*, transparent area) were measured. All experiments were performed in triplicate.

3. Results and discussion

We prepared the HP-β-CD and antibiotics aqueous mixtures by continuous mixing at room temperature for at least 2 h. The solutions were turbid in the presence of antibiotics, suggesting the formation of ICs between the CD and the antibiotics (Fig. S1a) [6]. We then electrospun the solutions, which formed nanofibrous mats of the HP-β-CD@antibiotics. Fig. S1b shows optical photos of the mats of the electrospun aqueous HP-β-CD solutions containing antibiotics. The white mats had good flexibility and could be folded without developing cracks, demonstrating their free-standing nature. The high concentrations of hydrogen bonds between the HP-β-CD molecules helped to maintain the fiber structure, even when folded [10].

We produced HP-β-CD fibers at concentrations of 180% (w/v), which is in the same range as electrospun aqueous HP-β-CD solutions previously reported in the literature [26]. Bead-free fibers with a smooth fiber texture were formed at a concentration of 180% (w/v). In contrast, beaded fibers were formed at 160%. The fiber diameters of the HP-β-CD nanofibers electrospun varied depending on the incorporated antibiotic (Fig. 2). The texture of

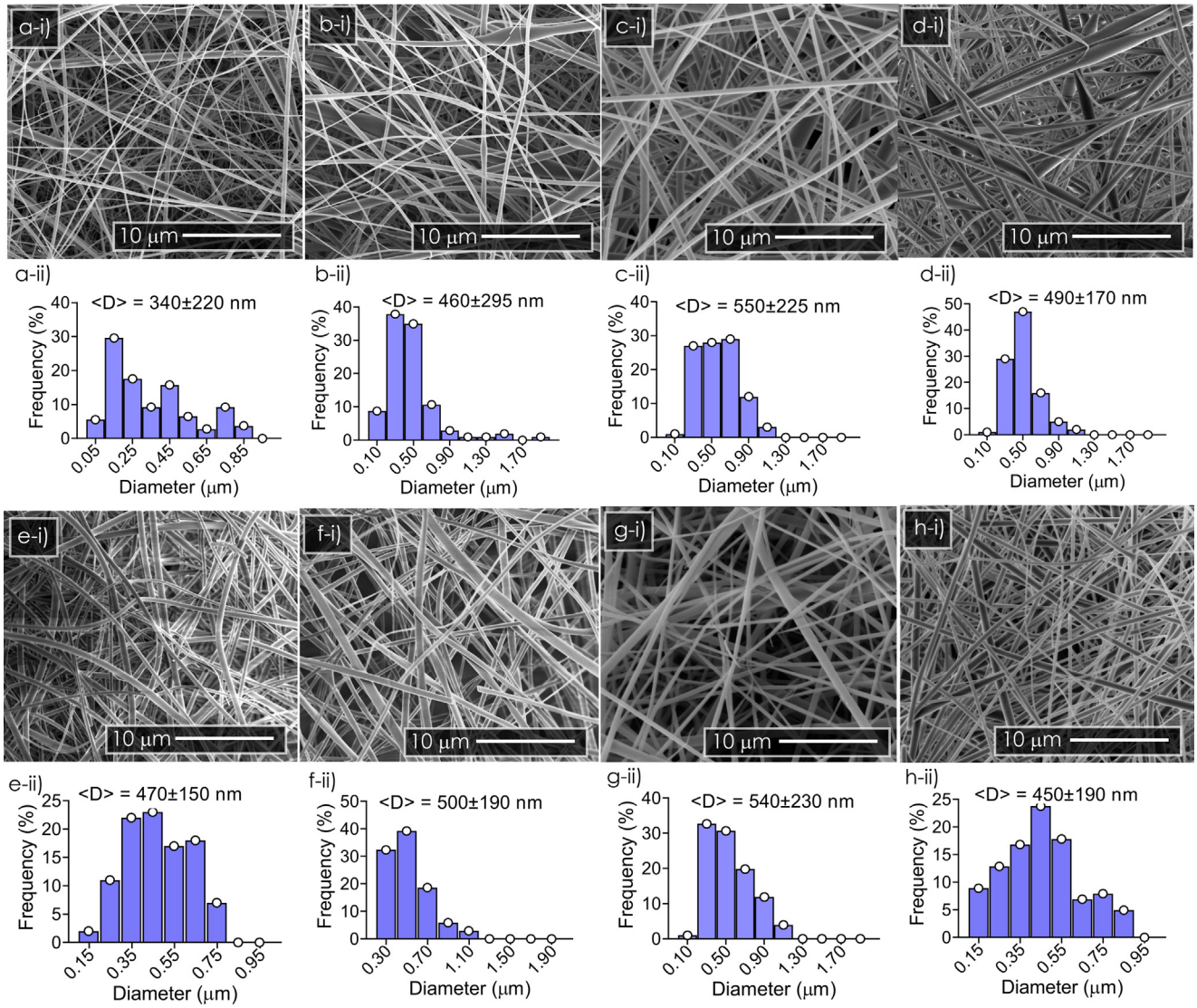

Fig. 2. Scanning electron micrographs of the HP-β-CD@antibiotics fibers produced at 1:1 (a-d) stoichiometry: (a-i) HP-β-CD@AMP, (b-i) HP-β-CD@CAP, (c-i) HP-β-CD@GEN, and (d-i) HP-β-CD@KAN. The statistical diameter distributions of the respective fibers are shown between (a-ii) and (d-ii). Scanning electron micrographs of the HP-β-CD@antibiotics fibers and pristine HP-β-CD fibers produced at 1:0.05 (e-h) stoichiometry (e-i) HP-β-CD@AMP, (f-i) HP-β-CD@CAP, and (g-i) HP-β-CD@GEN, and (h-i) HP-β-CD@KAN. The statistical diameter distributions of the respective fibers are shown between e-ii and h-ii.

the HP-β-CD@antibiotic fibers was smooth without any apparent porous surface texture. The mean diameters of the fibers prepared in the presence of AMP, CAP, GEN, and KAN at 1:1 stoichiometry were 340 ± 220, 460 ± 295, 550 ± 225, and 490 ± 170 nm, respectively. The mean diameters of the fibers were slightly higher for the fibers with lower antibiotic content. The respective diameters were 470 ± 150, 500 ± 190, 540 ± 230, and 450 ± 190 nm for HP-β-CD@AMP, HP-β-CD@CAP, HP-β-CD@GEN, and HP-β-CD@KAN. This slight decrease in fiber diameter with increasing antibiotic content may be attributed to conductivity, which increases with increased levels of antibiotic.

FTIR analysis can demonstrate the formation of ICs because the host–guest interactions result in the disappearance, broadening, or shifting of the characteristic FTIR bands of the guest molecules present in the CD cavity. The FTIR spectrum of HP-β-CD shows a broad stretching band of hydroxyl groups on the primary and secondary faces of the cavity, while the vibrations of the C—C/C—O stretching and the antisymmetric stretching of the C—O—C glycosidic bridge appear between 1020 and 1150 cm^{-1} (Fig. 3). Because these zones are dominated by the HP-β-CD, the characteristic peaks of the guest molecules in the respective zones are masked by the host. The N—H stretching vibration peak around 1600 cm^{-1} is visible for both GEN and KAN powder that shifted to a higher frequency for the fibers, which can be attributed to their IC with HP-β-CD molecules. Likewise, the N—O stretching vibrations at around 1550 cm^{-1} (asymmetrical) and 1365 cm^{-1} (symmetrical) of CAP shift in the FTIR spectrum of the HP-β-CD@CAP fibers. The FTIR spectrum of AMP displays bands at 3250, 1690, and 1605 cm^{-1}, corresponding to the –OH vibration, the C=O stretching vibrations of the four-membered lactam rings, and the N—H bending of the primary amines, respectively (Fig. 3). Overall, the appearance and shift of the characteristic peaks of the antibiotics in the FTIR spectra of the IC fibers demonstrate their complexation with the CD molecules within the fibers.

We explored the formation of ICs between the antibiotics and the HP-β-CD *via* ^{1}H NMR analysis. Fig. 4 shows the ^{1}H NMR spectra of the antibiotics and HP-β-CD@antibiotic nanofibrous mats dissolved in DMF-d_7 (KAN and GEN-containing fibers) and D_2O (CAP and AMP fibers). The methyl protons of the hydroxypropyl group appeared at 1.1 ppm, while the backbone protons of the CD

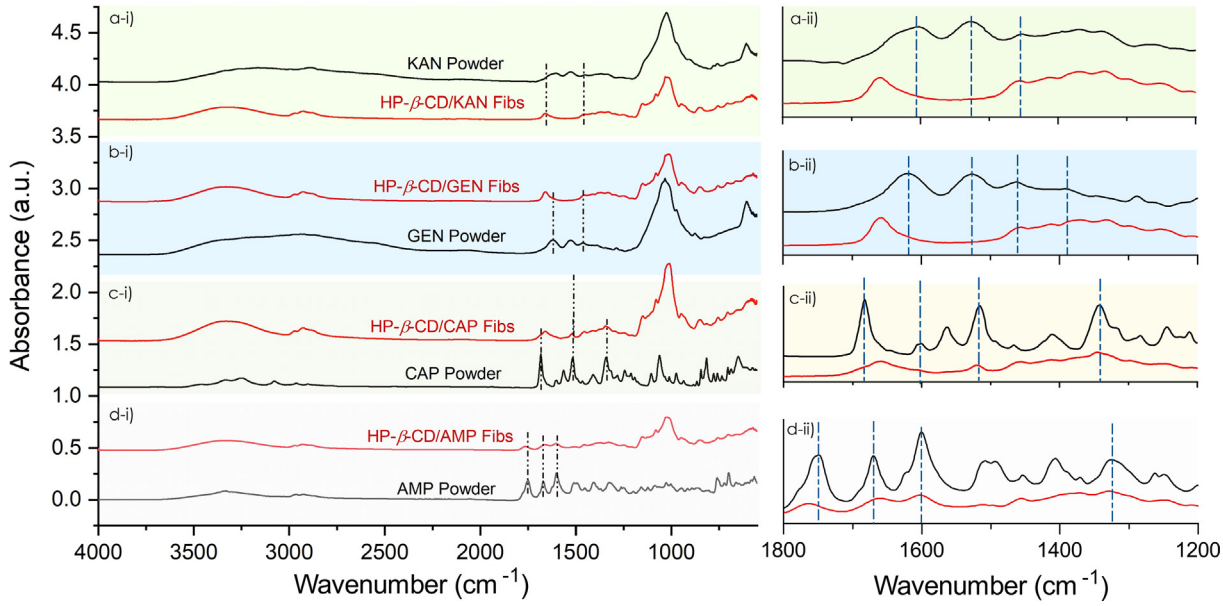

Fig. 3. FTIR spectra of the antibiotics and the nanofibrous mats upon inclusion complexation. The dashed lines correspond to the preserved characteristic bond vibrations of the antibiotics in the fibers. The nanofibers were produced at 180% (w/v) HP-β-CD. The molar ratio between HP-β-CD and the respective antibiotic is 1:1. The left panel shows the full range, while the right panel shows the narrow range of the respective FTIR spectra.

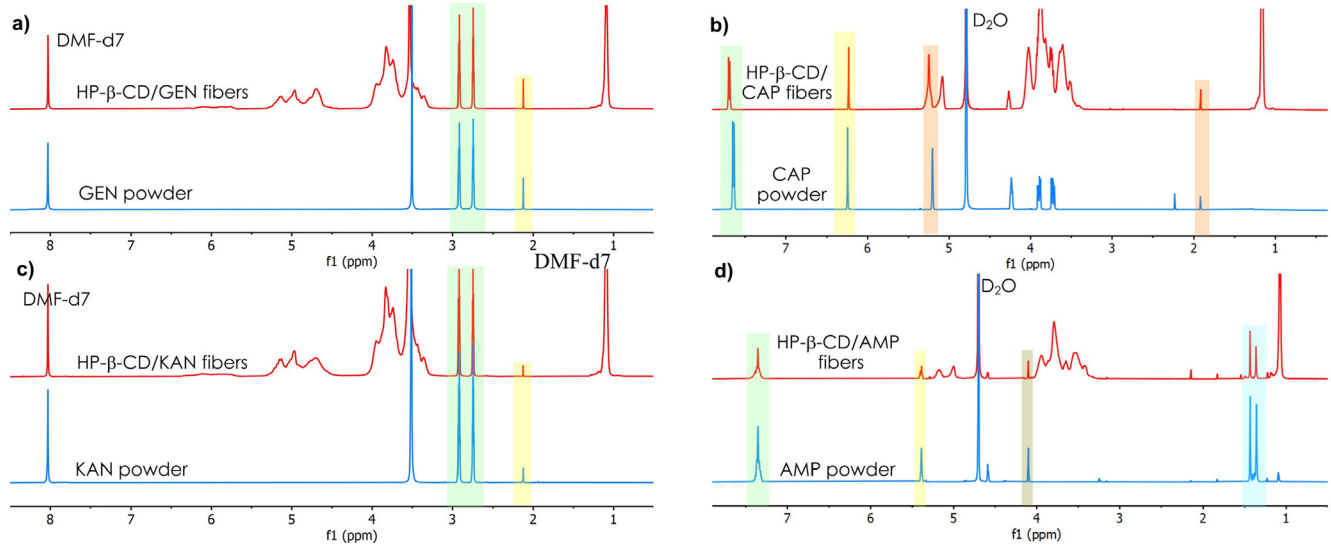

Fig. 4. ^{1}H NMR spectra of (a) GEN powder and HP-β-CD@GEN fibers, (b) CAP powder and HP-β-CD@CAP fibers, (c) KAN powder and HP-β-CD@KAN fibers, and (d) AMP powder and HP-β-CD@AMP fibers. The molar ratio between HP-β-CD and the respective antibiotic is 1:1.

appeared between 3.5 and 4.5 ppm. For the antibiotic-embedded CD fibers, the protons of the antibiotics in the ^{1}H NMR spectra of their respective fibers demonstrate their presence.

We explored the formation of ICs between the HP-β-CD and the antibiotics through thermal analyses of the fiber mats. Fig. 5 shows the TGA curves of the fiber mats composed of HP-β-CD@antibiotics and the pristine components. The decomposition of HP-β-CD takes place in two phases. In the first phase (300–380 °C), we observe a significant mass loss, followed by a second phase where a slow decomposition occurs. The thermal decomposition (T_d) temperature of the HP-β-CD is 356 °C, while the onset decomposition temperature is 313 °C. The antibiotics force the thermal decomposition temperature below 300 °C. The 1st derivative peak temperatures (Tp) are 216, 210, 210, and 265 °C for the pristine AMP, CAP, GEN, and KAN powders, respectively. The TGA curves of the HP-β-CD@antibiotic fibers show three transition zones. In the first zone, the mass loss at temperatures below 100 °C can be attributed to the adsorbed water, followed by the decomposition of antibiotics. The decomposition of the HP-β-CD molecule takes place between 300 and 550 °C. Since the sample does not have any inorganic component above 550 °C, no residue of the HP-β-CD remains. The presence of antibiotics significantly alters the decomposition pattern of the fibrous systems. In the case of the HP-β-CD@AMP fiber, the onset decomposition temperature increases to 280 °C. The onset decomposition temperature for HP-β-CD@CAP, HP-β-CD@GEN, and HP-β-CD@KAN are 265, 255, and 278 °C, respectively. All HP-β-CD@antibiotic fibers show a single transition thermal decomposition curve between 200 and 350 °C. The increased thermal stability of the antibiotics in the fibers demonstrates the formation of ICs.

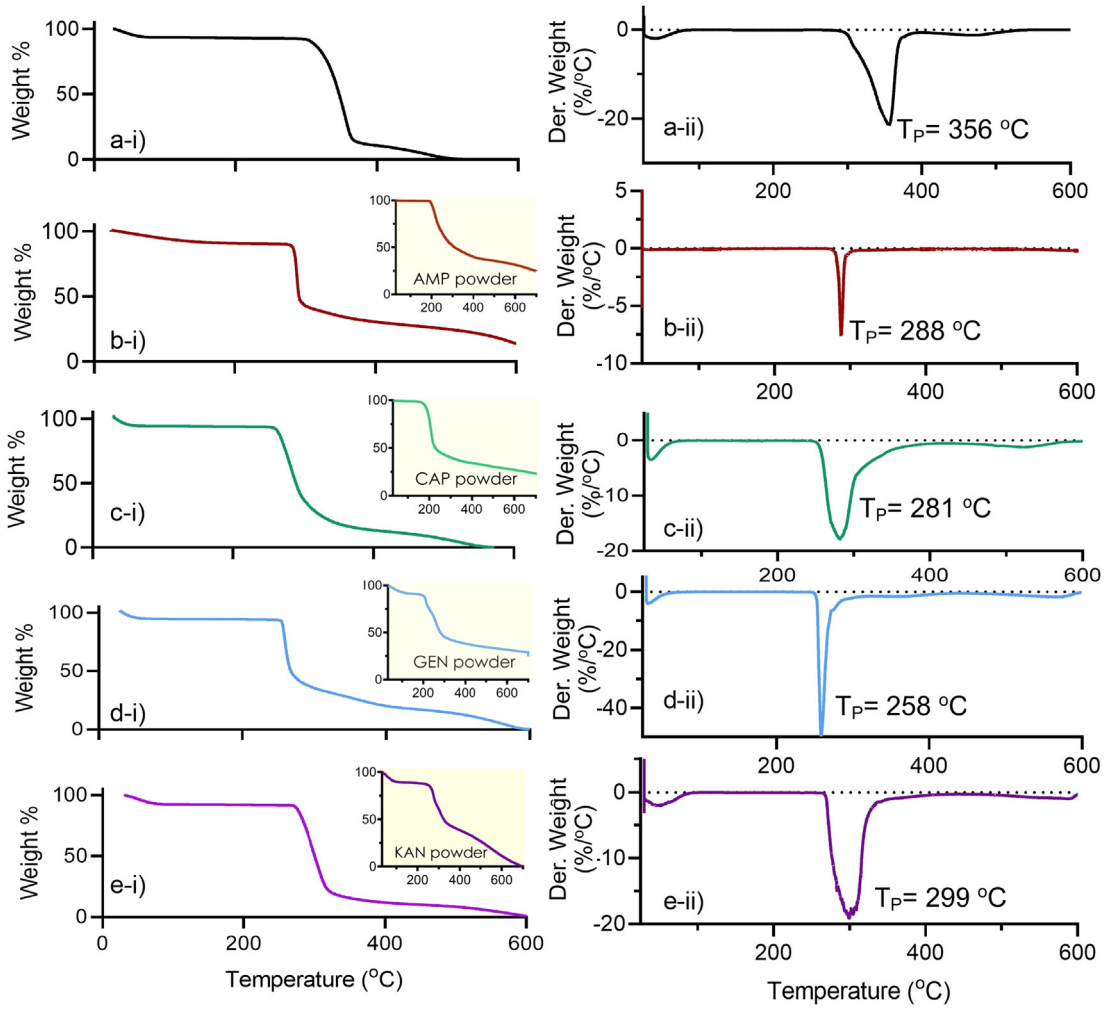

Fig. 5. TGA and differential TG thermograms of the HP-β-CD@antibiotics fibers and blank HP-β-CD fibers: (a) blank ($c_{HP\text{-}\beta\text{-}CD}$ = 180% (w/v)), (b) AMP ($c_{HP\text{-}\beta\text{-}CD}$ = 180% (w/v)), (c) CAP ($c_{HP\text{-}\beta\text{-}CD}$ = 180% (w/v)), (d) GEN ($c_{HP\text{-}\beta\text{-}CD}$ = 180% (w/v)), and (e) KAN ($c_{HP\text{-}\beta\text{-}CD}$ = 180% (w/v)). Insets show the thermograms of the respective antibiotics. The (i) series on the left show the thermograms of the HP-β-CD and HP-β-CD@antibitiotics fibers, and the (ii) series on the right show the first derivatives of the thermograms of the HP-β-CD and HP-β-CD@antibitiotics fibers.

The formation of ICs between the CD and antibiotics was also confirmed by XRD analysis. The disappearance of the crystalline peaks of the antibiotics upon complexation suggests the successful incorporation of the antibiotics into the host. We obtained XRD patterns of the antibiotics before and after electrospinning with CD (Fig. 6), where the antibiotics (AMP and CAP) showed highly crystalline peaks. However, after their complexation with the HP-β-CD and the electrospinning of their respective solutions, the crystalline peaks largely disappeared. The dominant crystalline peaks of AMP at 5.84° [15.11 Å], 15.81° [5.60 Å], 17,35° [5.10 Å], 19.84° [4.47 Å], and 23.25° [3.82 Å] disappeared in the IC fibers produced at a 1:1 molar ratio. Similarly, the crystalline peaks of CAP at 13.05° [6.77 Å], 15.85° [5.58 Å], 19.03° [4.65 Å], 20.79 [4.26 Å], 24.02° [3.70 Å], and 25.96° [3.42 Å] mostly disappeared. Even though very small peaks of the CAP were detectable for the fibers prepared at a 1:1 M ratio, those peaks were invisible for the fibers prepared using lower CAP content at 1:0.05 M ratio (Fig. 6b).

Overall, the absence of crystalline peaks of antibiotics in the fibers confirmed that there were no AMP crystals in the fibers (1:1), demonstrating the formation of IC fibers between the HP-β-CD and AMP. On the other hand, very small crystalline peaks of CAP were visible in the fibers (1:1), while these became invisible for the fibers prepared with lower antibiotic content (1:0.05). The overall crystalline nature of the antibiotics was lost due to their inclusion complexation with HP-β-CD molecules, as verified by the turbid appearance of the solutions of HP-β-CD and antibiotics (Fig. S1a).

Because of the hydrophilic and polymer-free structure, the HP-β-CD@antibiotic nanofibers rapidly dissolved in water. We carried out dissolution experiments of the electrospun mats on tissues wetted with artificial saliva (Fig. 7). Upon contact, the mats began to dissolve on the wet tissues, and the complete dissolution of the mats took only a few seconds. We observed a similar rapid dissolution trend for the HP-β-CD@AMP and HP-β-CD@CAP fibers. The dissolution time of the GEN-containing fibers was somewhat longer than the other HP-β-CD@antibiotic fibers. All of the fibers were immediately dissolved upon contact with the wet substrates, highlighting the potential use of the antibiotic-loaded CD nanofibers for oral drug delivery. Iversen et al. reported that switching from intravenously to orally administered antibiotics is as effective and safe as continued intravenous antibiotic treatment [27]. CDs are biocompatible, edible molecules that can be electrospun from water without the need for any polymer carrier. These characteristics underline the excellent potential for nanofibers to be employed for orally administered antibiotics.

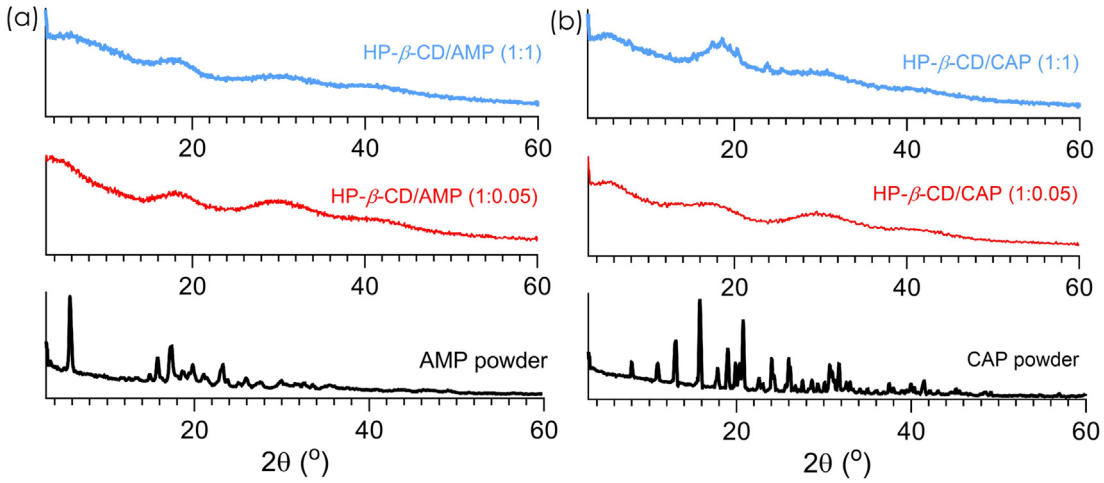

Fig. 6. Wide-angle XRD patterns of the antibiotics and inclusion-complexation nanofibers with HP-β-CD.

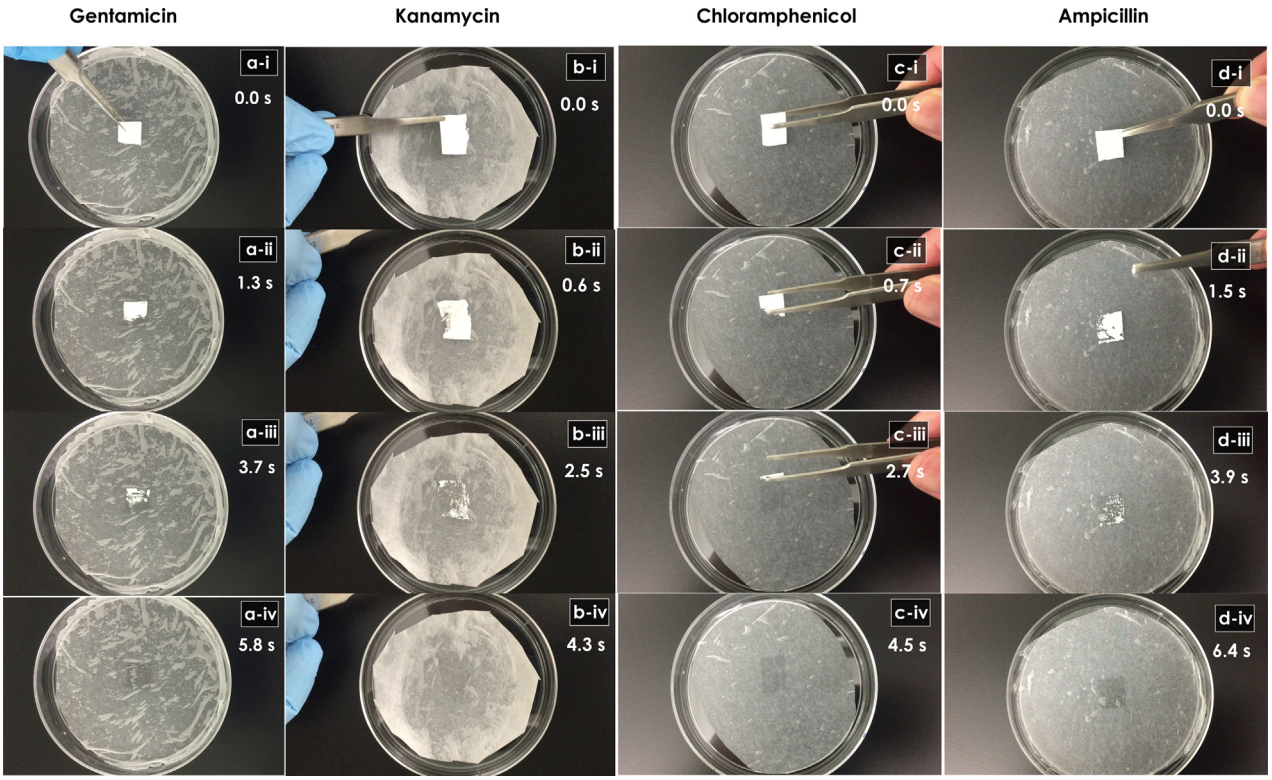

Fig. 7. Dissolution test for the HP-β-CD fibers containing GEN, KAN, CAP, and AMP. Dissolution tests were carried out using artificial saliva at room temperature. The images were taken from the respective dissolution test videos provided in the Supporting Information.

Molecular modeling studies can reveal the complexation between the antibiotics and the HP-β-CD (Fig. 8). We investigated the structural optimization of both the antibiotics and the HP-β-CD and their inclusion complexation in a vacuum and in water using a first-principles approach. We performed the inclusion-complexation modeling study using the orientation (head and tail) of the antibiotics with respect to the wide and narrow rim of the HP-β-CD. The complexation energy (E_{comp}) was calculated for the most favorable configurations using the formula in Eq-1. The calculated results for 1:1 stoichiometry for both the vacuum and water environment are summarized in Table 1. We found that the complexation energies depend on the structural orientation and the antibiotic molecule.

We observed the complexation energies for head-orientation, which followed the order of CAP > GEN > KAN > AMP covering the range of −36.6 to −14.8 kcal mol^{-1} in a vacuum, and GEN > KAN > CAP > AMP covering the range of −24.8 to −11.9 kc al mol^{-1} in water. These results were in line with the solubility of the antibiotics. GEN had the lowest water solubility of the antibiotics used and was thus more favorable for complexation with the HP-β-CD molecule. Moreover, these results were in line with the FTIR results of the nanofibrous mats, which revealed band shifts in the presence of HP-β-CD, demonstrating the formation of the inclusion complexes (see Fig. 3). The TGA analysis of the fibrous mats also revealed an increase in the degradation temperatures of the antibiotics in the CD fibers, demonstrating the formation of

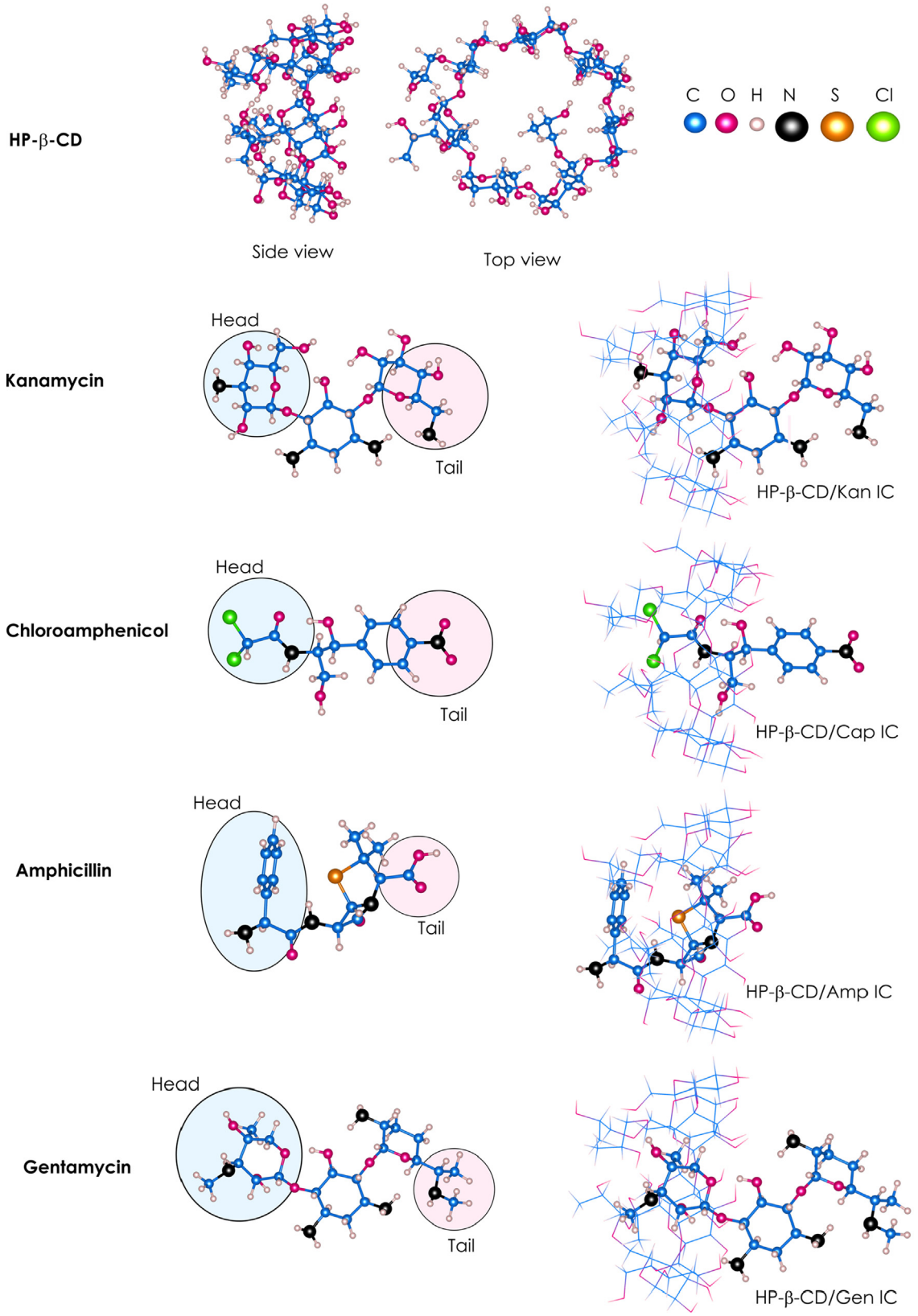

Fig. 8. Molecular simulation for the inclusion complexation of HP-β-CD with antibiotics. The complexation energy of the respective inclusion complexation in a vacuum and in water is given in Table 1.

inclusion complexation. We also calculated the solvation energies in water according to the formula in Eq-2, where E_{water} and E_{vacuum} are the total energies of IC (or HP-β-CD:antibiotics-IC) in a solvent and vacuum, respectively. E_{solv} does not indicate absolute solubility, but it reveals the solubility trend. The respective E_{solv} values for the complexes are listed in Table 1.

Table 1
Complexation and solvation energies (kcal mol^{-1}) of the inclusion complexes of antibiotics with HP-β-CD from different geometries in a vacuum and in water.

	E_{comp}^{vacuum}		E_{comp}^{water}		E_{sol}
	IC from head	IC from tail	IC from head	IC from tail	IC from head
HP-β-CD@KAN IC	−25.39	−22.38	−16.77	ND	8.61
HP-β-CD@CAP IC	−36.64	−16.12	−17.53	ND	19.11
HP-β-CD@AMP IC	−14.84	−12.79	−11.99	ND	2.85
HP-β-CD@GEN IC	−36.37	−21.52	−24.89	ND	11.48

ND: Not determined.

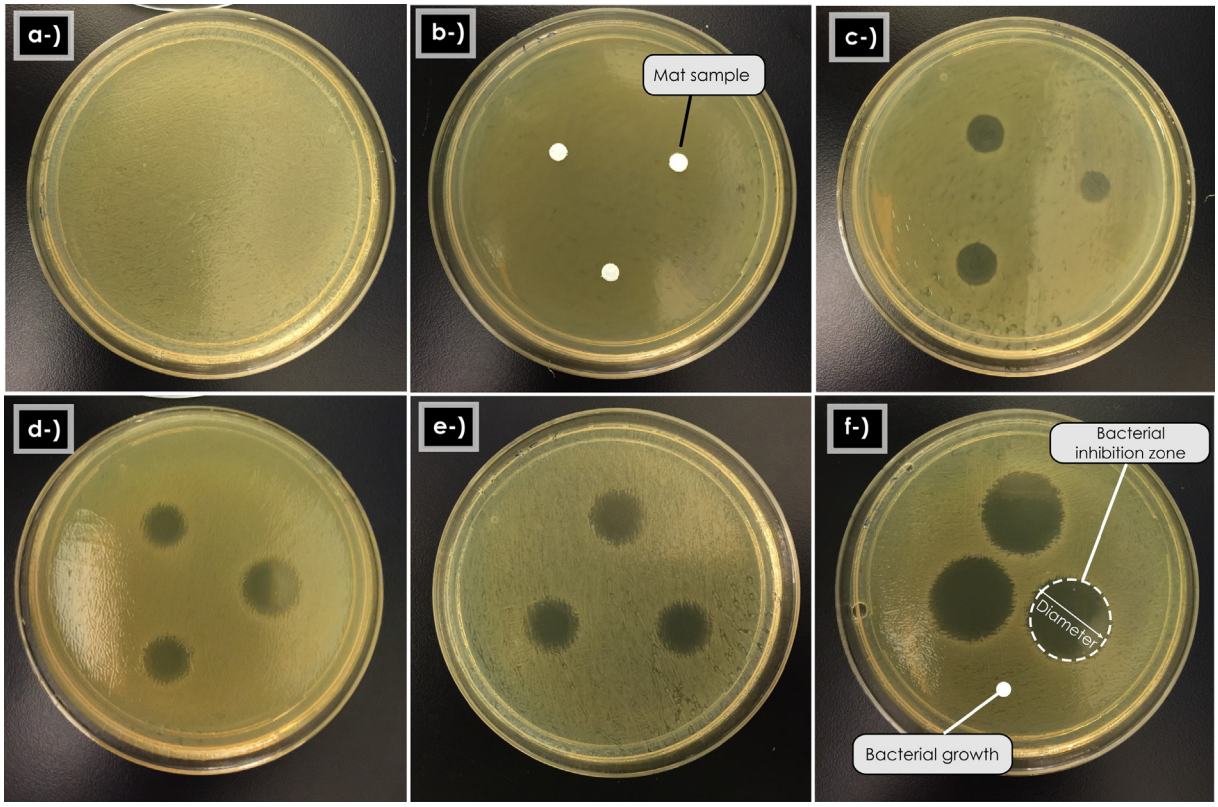

Fig. 9. Antibacterial activity of the HP-β-CD@antibiotic nanofibrous mats against *E. coli* through a disk-diffusion assay: (a) pristine HP-β-CD fibers; (b) control, water-insoluble polyimide fibers showing the initial diameter of the mats; (c) HP-β-CD@AMP fibers (1:0.05), (d) HP-β-CD@KAN fibers(1:0.05), (e) HP-β-CD@GEN fibers (1:0.05), and (f) HP-β-CD@AMP fibers (1:1). Treatment time is 24 h at 37 °C.

We explored the antibacterial activity of the fibers through a disk-diffusion assay using Gram-negative bacteria (*E. coli*). Fig. 9 shows the *E. coli*-seeded agar Petri dishes after exposure to fibers for 24 h. The pristine HP-β-CD did not exhibit any antibacterial activity, and thus we did not observe any bacterial-inhibition zone (Fig. 9a). We used water-insoluble polyimide fibers as a negative control to show the sample size (Fig. 9b). As expected, we did not observe any inhibition zone around the control sample because it did not have any antibacterial activity. However, the HP-β-CD@antibiotic nanofibers (1:0.05) showed obvious transparent circles due to the inhibition of *E. coli* growth in this region. The external diameters of the circles were 13.99 ± 0.32 mm for HP-β-CD@GEN, 12.66 ± 1.79 mm for HP-β-CD@KAN, 8.98 ± 1.45 m m for HP-β-CD@AMP, and 0 for HP-β-CD@CAP (Table 2). The HP-β-CD@AMP fiber prepared at a 1:1 molar ratio revealed an external diameter of 21.18 ± 0.43 mm. We observed the highest antibacterial activity for the fibers containing GEN, followed by KAN and then AMP. The fibers containing CAP did not exhibit any inhibition owing to the CAP resistance of the used *E. coli* strain. Even though the loadings of antibiotics were relatively low, we

Table 2
Diameters of bacterial inhibition rings for the HP-β-CD@antibiotics nanofibers with different encapsulated drug contents. Sample diameter: 4.54 ± 0.05 mm; n.a. = not applicable.

Samples	HP-β-CD@antibiotic (mol:mol)	External diameter (mm)	Diameter difference (mm)
HP-β-CD	n.a.	0	− 4.54 ± 0.1
HP-β-CD@GEN	1:0.05	13.99 ± 0.3	9.45 ± 0.2
HP-β-CD@KAN	1:0.05	12.66 ± 1.8	8.12 ± 1.5
HP-β-CD@AMP	1:0.05	8.98 ± 1.4	4.44 ± 1.3
HP-β-CD@CAP	1:0.05	0	− 4.54 ± 0.1
HP-β-CD@AMP	1:1	21.18 ± 0.4	16.64 ± 0.4

attributed the high antibacterial activity of the fibers to the high potency antibacterial activity of the antibiotics.

Drug-loaded CD nanofibers that have been described in the literature to date mostly suffer from an inability to carry large amounts of drugs, typically less than 10 wt% [28,29], and furthermore, these studies mainly focused on a single drug molecule. In our work, CD nanofibers with high antibiotic content were produced through the electrospinning of aqueous IC solutions, and four different antibiotics with high potency were investigated. Good antibiotic encapsulation (45–90%) was observed by TGA analysis. These fast-dissolving nanofibers have great potential to be used for oral administration of antibiotics. Furthermore, CDs self-assemble in water, forming aggregates bound by mainly hydrogen bonds. The electrospinning of such aggregates could produce continuous fibers, and the concept presented here could be employed for other aggregates with a high hydrogen-bonding potential. Since the resulting fibers are composed of hydrophilic CD aggregates, the surface of the fibers starts to dissolve upon contact with water, dissolving the complete fibrous mat within seconds.

4. Conclusions

Compared to previously reported approaches that were limited to low drug loadings [28,29], the present research demonstrates the formulation of CD nanofibers with high drug loadings. Bead-free CD nanofibers with high antibiotic loadings were produced through the electrospinning of cyclodextrin-antibiotic inclusion complexes from water. ^{1}H NMR and XRD analysis confirmed the inclusion complexation between the HP-β-CD and the antibiotics with the appearance of proton peaks of antibiotics in the spectra of the nanofibers and disappearance of crystalline peaks in the X-ray diffraction patterns, respectively. Likewise, FTIR analyses confirmed the presence of antibiotics in the fibers. The *ab initio* computational studies revealed that the HP-β-CD preferably hosts antibiotics from the head side. The highest complexation energy in a vacuum was for CAP, followed by GEN > KAN > AMP, while in water, the order followed GEN > CAP > KAN > AMP. The formulations showed good antibiotic encapsulation (45–90%). The nanofibrous mats successfully demonstrated high antibacterial activity in a disk-diffusion assay, inhibiting the growth of Gram-negative *E. coli*. We found the highest antibacterial activity for HP-β-CD@GEN, followed by HP-β-CD@KAN, and then HP-β-CD@AMP fibers. The hydrophilic and uncross-linked nature of these fibers allows for their rapid dissolution in water and artificial saliva (within a few seconds), thus releasing the antibiotics. Our findings highlight the potential use of polymer-free cyclodextrin-antibiotic nanofibers as fast-dissolving oral drug delivery devices and orally administered antibiotics. Unlike many reported studies with low drug loadings, the presented concept allows high drug loadings. Therefore, it has great potential to be employed for oral drug delivery of poorly water-soluble drugs. A similar concept can be applied by incorporating antiviral molecules with further chemical cross-linking to produce stable antiviral nanofibrous materials to develop antiviral nanofibrous masks.

5. Data availability

The data that support the findings of this study are available from the corresponding author upon reasonable request.

CRediT authorship contribution statement

Fuat Topuz: Conceptualization, Investigation, Formal analysis, Writing - original draft. **Mehmet E. Kilic:** Investigation. **Engin Durgun:** Investigation. **Gyorgy Szekely:** Conceptualization, Funding acquisition, Supervision, Writing - review & editing.

Declaration of Competing Interest

The authors declare that they have no known competing financial interests or personal relationships that could have appeared to influence the work reported in this paper.

Acknowledgments

The postdoctoral fellowship from King Abdullah University of Science and Technology (KAUST) is gratefully acknowledged (FT). The research reported in this publication was supported by funding from KAUST.

Appendix A. Supplementary material

Supplementary data to this article can be found online at https://doi.org/10.1016/j.jcis.2020.11.072.

References

[1] J. Szejtli, Introduction and general overview of cyclodextrin chemistry, Chem. Rev. 98 (5) (1998) 1743–1754.
[2] F. Topuz, T. Uyar, Electrospinning of cyclodextrin functional nanofibers for drug delivery applications, Pharmaceutics 11 (1) (2019) 6.
[3] T. Loftsson, D. Hreinsdóttir, M. Másson, Evaluation of cyclodextrin solubilization of drugs, Int. J. Pharm. 302 (1) (2005) 18–28.
[4] A. Domokos, A. Balogh, D. Dénes, G. Nyerges, L. Ződi, B. Farkas, G. Marosi, Z.K. Nagy, Continuous manufacturing of orally dissolving webs containing a poorly soluble drug via electrospinning, Eur. J. Pharm. Sci. 130 (2019) 91–99.
[5] A. Balogh, T. Horváthová, Z. Fülöp, T. Loftsson, A.H. Harasztos, G. Marosi, Z.K. Nagy, Electroblowing and electrospinning of fibrous diclofenac sodium-cyclodextrin complex-based reconstitution injection, J. Drug Delivery Sci. Technol. 26 (2015) 28–34.
[6] A. Celebioglu, T. Uyar, Fast dissolving oral drug delivery system based on electrospun nanofibrous webs of cyclodextrin/ibuprofen inclusion complex nanofibers, Mol. Pharm. 16 (10) (2019) 4387–4398.
[7] F. van de Manakker, T. Vermonden, C.F. van Nostrum, W.E. Hennink, Cyclodextrin-based polymeric materials: synthesis, properties, and pharmaceutical/biomedical applications, Biomacromolecules 10 (12) (2009) 3157–3175.
[8] J. Zhang, P.X. Ma, Cyclodextrin-based supramolecular systems for drug delivery: recent progress and future perspective, Adv. Drug Deliv. Rev. 65 (9) (2013) 1215–1233.
[9] R. Gref, C. Amiel, K. Molinard, S. Daoud-Mahammed, B. Sébille, B. Gillet, J.-C. Beloeil, C. Ringard, V. Rosilio, J. Poupaert, P. Couvreur, New self-assembled nanogels based on host–guest interactions: characterization and drug loading, J. Control. Release 111 (3) (2006) 316–324.
[10] J.L. Manasco, C.D. Saquing, C. Tang, S.A. Khan, Cyclodextrin fibers via polymer-free electrospinning, RSC Adv. 2 (9) (2012) 3778–3784.
[11] M. Allais, D. Mailley, P. Hébraud, D. Ihiawakrim, V. Ball, F. Meyer, A. Hébraud, G. Schlatter, Polymer-free electrospinning of tannic acid and cross-linking in water for hybrid supramolecular nanofibres, Nanoscale 10 (19) (2018) 9164–9173.
[12] H.S. Yu, J.M. Lee, Y.S. Youn, K.T. Oh, K. Na, E.S. Lee, γ-Cyclodextrin-phenylacetic acid mesh as a drug trap, Carbohydr. Polym. 184 (2018) 390–400.
[13] F. Topuz, T. Uyar, Atomic layer deposition of palladium nanoparticles on a functional electrospun poly-cyclodextrin nanoweb as a flexible and reusable heterogeneous nanocatalyst for the reduction of nitroaromatic compounds, Nanoscale Adv. 1 (10) (2019) 4082–4089.
[14] R. Zhao, Y. Wang, X. Li, B. Sun, C. Wang, Synthesis of β-cyclodextrin-based electrospun nanofiber membranes for highly efficient adsorption and separation of methylene blue, ACS Appl. Mater. Interfaces 7 (48) (2015) 26649–26657.
[15] S. Saffarionpour, Nanoencapsulation of hydrophobic food flavor ingredients and their cyclodextrin inclusion complexes, Food Bioprocess Technol. 12 (7) (2019) 1157–1173.
[16] H. Bender, A bacterial glucoamylase degrading cyclodextrins, Eur. J. Biochem. 115 (2) (1981) 287–291.
[17] A. Celebioglu, O.C.O. Umu, T. Tekinay, T. Uyar, Antibacterial electrospun nanofibers from triclosan/cyclodextrin inclusion complexes, Colloids Surf., B 116 (2014) 612–619.
[18] G. Kresse, J. Furthmüller, Efficient iterative schemes for ab initio total-energy calculations using a plane-wave basis set, Phys. Rev. B 54 (16) (1996) 11169–11186.

[19] G. Kresse, J. Furthmüller, Efficiency of ab-initio total energy calculations for metals and semiconductors using a plane-wave basis set, Comput. Mater. Sci. 6 (1) (1996) 15–50.
[20] W. Kohn, L.J. Sham, Self-consistent equations including exchange and correlation effects, Phys. Rev. 140 (4A) (1965) A1133–A1138.
[21] P. Hohenberg, W. Kohn, Inhomogeneous electron gas, Phys. Rev. 136 (3B) (1964) B864–B871.
[22] J.P. Perdew, K. Burke, M. Ernzerhof, Generalized gradient approximation made simple, Phys. Rev. Lett. 77 (18) (1996) 3865–3868.
[23] S. Grimme, Semiempirical GGA-type density functional constructed with a long-range dispersion correction, J. Comput. Chem. 27 (15) (2006) 1787–1799.
[24] P.E. Blöchl, Projector augmented-wave method, Phys. Rev. B 50 (24) (1994) 17953–17979.
[25] K. Mathew, R. Sundararaman, K. Letchworth-Weaver, T.A. Arias, R.G. Hennig, Implicit solvation model for density-functional study of nanocrystal surfaces and reaction pathways, J. Chem. Phys. 140 (8) (2014) 084106.
[26] F. Topuz, T. Uyar, Electrospinning of nanocomposite nanofibers from cyclodextrin and laponite, Compos. Commun. 12 (2019) 33–38.
[27] K. Iversen, N. Ihlemann, S.U. Gill, T. Madsen, H. Elming, K.T. Jensen, N.E. Bruun, D.E. Høfsten, K. Fursted, J.J. Christensen, M. Schultz, C.F. Klein, E.L. Fosbøll, F. Rosenvinge, H.C. Schønheyder, L. Køber, C. Torp-Pedersen, J. Helweg-Larsen, N. Tønder, C. Moser, H. Bundgaard, Partial oral versus intravenous antibiotic treatment of endocarditis, N. Engl. J. Med. 380 (5) (2018) 415–424.
[28] Z.I. Yildiz, A. Celebioglu, M.E. Kilic, E. Durgun, T. Uyar, Fast-dissolving carvacrol/cyclodextrin inclusion complex electrospun fibers with enhanced thermal stability, water solubility, and antioxidant activity, J. Mater. Sci. 53 (23) (2018) 15837–15849.
[29] A. Celebioglu, T. Uyar, Fast-dissolving antioxidant curcumin/cyclodextrin inclusion complex electrospun nanofibrous webs, Food Chem. 317 (2020) 126397.